Am J Cancer Res 2023;13(9):4057-4072
www.ajcr.us /ISSN:2156-6976/ajcr0150912

Original Article

Anticancer peptides from induced tumor-suppressing cells for inhibiting osteosarcoma cells

Chang-Peng Cui[1,2], Qing-Ji Huo[1,2], Xue Xiong[1,2], Ke-Xin Li[1,2], Peng Ma[3], Gui-Fen Qiang[3], Pankita H Pandya[4,5], Mohammad R Saadatzadeh[4,5], Khadijeh Bijangi Vishehsaraei[6], Melissa A Kacena[4,7,8], Uma K Aryal[9], Karen E Pollok[4,5], Bai-Yan Li[1], Hiroki Yokota[2,4,8]

[1]Department of Pharmacology, School of Pharmacy, Harbin Medical University, Harbin 150081, Heilongjiang, China; [2]Department of Biomedical Engineering, Indiana University Purdue University Indianapolis, Indianapolis, IN 46202, USA; [3]State Key Laboratory of Bioactive Substance and Function for Natural Medicines, Institute of Materia Medica, Chinese Academy of Medical Sciences and Peking Union Medical College and Beijing Key Laboratory of Drug Target and Screening Research, Beijing 100050, China; [4]Indiana University Simon Comprehensive Cancer Center, Indiana University School of Medicine, Indianapolis, IN 46202, USA; [5]Department of Pediatrics, Indiana University School of Medicine, Indianapolis, IN 46202, USA; [6]Department of Pediatric Hematology and Oncology, Indiana University School of Medicine, Indianapolis, IN 46202, USA; [7]Department of Orthopaedic Surgery, Indiana University School of Medicine, Indianapolis, IN 46202, USA; [8]Indiana Center for Musculoskeletal Health, Indiana University School of Medicine, Indianapolis, IN 46202, USA; [9]Department of Basic Medical Sciences, Interdisciplinary Biomedical Sciences Program, Purdue University, West Lafayette, IN 47907, USA

Received April 25, 2023; Accepted August 9, 2023; Epub September 15, 2023; Published September 30, 2023

Abstract: Osteosarcoma (OS) is the most frequent primary bone cancer, which is mainly suffered by children and young adults. While the current surgical treatment combined with chemotherapy is effective for the early stage of OS, advanced OS preferentially metastasizes to the lung and is difficult to treat. Here, we examined the efficacy of ten anti-OS peptide candidates from a trypsin-digested conditioned medium that was derived from the secretome of induced tumor-suppressing cells (iTSCs). Using OS cell lines, the antitumor capabilities of the peptide candidates were evaluated by assaying the alterations in metabolic activities, proliferation, motility, and invasion of OS cells. Among ten candidates, peptide P05 (ADDGRPFPQVIK), a fragment of aldolase A (ALDOA), presented the most potent OS-suppressing capabilities. Its efficacy was additive with standard-of-care chemotherapeutic agents such as cisplatin and doxorubicin, and it downregulated oncoproteins such as epidermal growth factor receptor (EGFR), Snail, and Src in OS cells. Interestingly, P05 did not present inhibitory effects on non-OS skeletal cells such as mesenchymal stem cells and osteoblast cells. Collectively, this study demonstrated that iTSC-derived secretomes may provide a source for identifying anticancer peptides, and P05 may warrant further evaluations for the treatment of OS.

Keywords: Osteosarcoma, peptide, ALDOA, EGFR, induced tumor-suppressing cells

Introduction

Osteosarcoma (OS) is a primary bone cancer that affects mostly children and young adults [1, 2]. Its common site of induction is the lower limb, and the standard-of-care treatment includes chemotherapy as well as surgical removal [3, 4]. Popular MAP chemotherapy with three chemotherapeutic agents, including methotrexate, doxorubicin, and cisplatin, is effective in inhibiting its progression and recurrence [5, 6]. However, advanced OS tends to metastasize, most often to the lung, and it is difficult to treat metastasized OS [7, 8]. The development of effective treatment, as well as early detection, is essential for improving the survival of patients with advanced OS.

Anticancer peptides (ACPs), a series of peptides approximately with 10-60 amino acids, have recently emerged as a promising therapeutic choice for many types of cancer, potentially, because of their high penetration and specificity with fewer side effects [9-12]. Compared to

tumor-suppressing proteins, peptides are generally easier to synthesize and are considered less likely to cause drug resistance [13, 14], although they may have drawbacks in their stability with a short half-life [15, 16]. Several computational approaches have been developed to predict the anticancer activities of ACP candidates [17-19], but it is still a challenge to design effective ACPs since a variety of mechanisms of anticancer action are considered [20].

For the treatment of OS, we herein selected ACP candidates and examined their tumor-suppressive capabilities. The ten ACP candidates were derived from tumor-suppressing proteins that were secreted from a unique type of cells named induced tumor-suppressing cells (iTSCs) [21-26]. We have shown that the activation of cMyc paradoxically converts cancer cells as well as non-cancer cells into iTSCs, and iTSC-derived conditioned medium (CM) is enriched with tumor-suppressing proteins such as Calreticulin, Enolase 1, and Moesin [24, 27]. The question we addressed here was whether effective ACPs can be generated from proteins that were enriched in iTSC-derived CM. To the best of our knowledge, little is known about ACPs that are effective for the treatment of OS.

The generation of iTSCs by activating oncogenic signaling, such as cMyc and β-catenin/Wnt signaling, is linked to an unsuccessful reprogramming of induced pluripotent stem cells (iPSCs) [28-30]. To produce iPSCs, the transfection of the four transcription factors such as cMyc, Oct4, Klf4, and Sox2 is necessary [31]. Importantly, however, the successful reprogramming rate of adult somatic cells is only about 1%, and a majority of transfected cells fail to acquire pluripotency [32]. One type of such unsuccessfully transfected cells becomes oncogene-induced senescent (OIS) cells that secrete tumor-suppressive proteins [33]. While it is unclear whether all iTSCs are senescent, mounting evidence suggests that the overexpression of oncoproteins and the activation of oncogenic pathways facilitate the secretion of anti-cancer proteins [22].

In this study, we created trypsin-digested peptides using iTSC-derived CM and selected the ten ACP candidates (P01 to P10) that were highly expressed in the peptide pool. After the prescreening of these candidates, we selected peptide P05 as the most potent ACP for further characterization. P05 was derived from aldolase A (ALDOA), which is a glycolytic enzyme responsible for converting fructose-1,6-bisphosphate to glyceraldehyde 3-phosphate and dihydroxyacetone phosphate [34]. The levels of glycolytic enzymes, including ALDOA, are generally elevated in cancer cells [35, 36], and they contribute to inducing the Warburg effect. Accordingly, cancer cells preferentially use glycolysis rather than oxidative phosphorylation for energy production. Importantly, we have shown that extracellular ALDOA, which is enriched in iTSC-derived CM, acts as a tumor-suppressing protein in breast cancer [37]. In this study, we presented that ACPs can be identified from iTSC-derived tumor-suppressing proteins, and ALDOA-derived P05 is a potential candidate for the treatment of OS.

Materials and methods

Cell culture

Human OS cell lines such as MG63 [38] and U2OS [39] (86051601-1VL and 92022711-1VL, Sigma, St. Louis, MO, USA), a patient-derived xenograft (PDX) TT2-77 OS xenoline [40], murine K7M2 osteosarcoma cancer cells [41] (ATCC, Manassas, VA, USA), RAW264.7 pre-osteoclast cells (ATCC), and murine mesenchymal stem cells (MSCs) derived from the bone marrow of the C57BL/6 strain were cultured in DMEM. MC3T3-E1 osteoblasts (Sigma) were grown in αMEM (Gibco, Carlsbad, CA, USA), and human fetal osteoblast (hFOB) (ATCC) were grown in DMEM. The culture medium was supplemented with 10% fetal bovine serum and antibiotics (100 units/mL penicillin, and 100 μg/mL streptomycin; Life Technologies, Grand Island, NY, USA). Cells were maintained at 37°C and 5% CO_2.

OS cells were treated with 10 peptides (P01 to P10, Genscript Biotech, Piscataway, NJ, USA) and chemotherapeutic agents, such as Taxol (#1097, Tocris Bioscience, Minneapolis, MN, USA), Doxorubicin (#2252, Tocris Bioscience), and Cisplatin (#2251, Tocris Bioscience). TT2 OS cells were also treated with human recombinant ALDOA protein (#MBS8248528, MyBioSource, San Diego, CA, USA). For *in vitro* experiments, CM was prepared using low-speed centrifugation at 2,000 rpm for 10 min. The supernatants were further centrifuged at 4,000 rpm for 10 min and subjected to filtra-

tion with a 0.22-μm polyethersulfone membrane (Sigma).

MTT assay and EdU assay

MTT-based metabolic activity was evaluated using ~2,000 cells seeded in 96-well plates. Cells were incubated for two days with treatment agents. They were dyed with 0.5 mg/mL thiazolyl blue tetrazolium bromide (#M5655, Sigma) on day 4, and a mixed solution of isopropyl alcohol and hydrochloric acid was added at the ratio of 60:1. Optical density for assessing metabolic activities was determined at 562 nm. EdU-based proliferation activity was evaluated using ~1,000 cells, which were seeded in 96-well plates. We employed a fluorescence-based cell proliferation kit (Click-iT™, EdU Alexa Fluor™ 488 Imaging Kit; Thermo Fisher, Waltham, MA, USA), using the procedure described by the manufacturer.

Scratch assay

A wound-healing scratch assay was utilized to evaluate the two-dimensional migratory behavior of OS cells by determining the change in the scratch area. Approximately 3×10^5 cells were seeded in 12-well plates on day 1. On day 2, a scratch was made on the cell layer with a tip of a plastic pipette. Cells were washed with DMEM to remove floating cells. Images of cell-free zones were taken at 0 h and 24 h with a light microscope (40×), and the areas of the cell-free zone were quantified by Image J.

Transwell invasion assay

The invasion capacity of tumor cells was determined using a 12-well plate and transwell chambers (#353182, Thermo Fisher) with 8-μm pore size. The chambers were coated with 300 μL Matrigel (100 μg/mL), and 500 μL of the serum-free medium was added. The chamber was washed three times with the serum-free medium. Approximately 7×10^4 cells in 300 μL serum-free DMEM were placed in the upper chamber, and 800 μL CM was added to the lower chamber. Cells, which invaded the lower side of the membrane, were fixed, and stained with methanol and crystal violet. Five randomly chosen images were taken with an inverted optical microscope (100×), and the average number of stained cells, which represented the invasion capacity, was determined.

Western blot analysis

Cells were lysed with a RIPA lysis buffer (#sc-24948, Santa Cruz Biotechnology, Dallas, TX, USA) with protease inhibitors (#PIA32963, Thermo Fisher), and phosphatase inhibitors (#2006643, Cal-biochem, Billerica, MA, USA). Proteins were separated by 10%-15% SDS gel (Bio-Rad Laboratories, Hercules, CA, USA) and transferred to a polyvinylidene difluoride membrane (#IPVH00010, Millipore, Billerica, MA, USA). The membrane was incubated with the primary antibodies, followed by incubation with secondary antibodies (#7074S/7076S, Cell Signaling, Danvers, MA, USA). We used antibodies against EGFR, ALDOA, Snail, p-Src, Src, cleaved caspase 3, caspase 3, IL-1β, IL-6 (Cell Signaling), and M-CSF, OPN (Santa Cruz Biotechnology), with β-actin (Sigma) as a control. The protein level was determined using a SuperSignal west femto maximum sensitivity substrate (#PI34096, Thermo Fisher), and a luminescent image analyzer (#LAS-3000, Fuji Film, Tokyo, Japan) was used to quantify signal intensities [42].

Plasmid transfection and RNA interference

The overexpression of ALDOA was conducted by transfecting plasmids (#109854; Addgene, Cambridge, MA, USA), while blank plasmids (FLAG-HA-pcDNA3.1; Addgene) were used as a control. RNA interference was conducted using siRNA specific to EGFR (#AM16708; Thermo Fisher) with a negative siRNA (Silencer Select #1, Thermo Fisher) as a nonspecific control using the procedure previously described [43].

Immunoprecipitation

Immunoprecipitation was conducted with an immunoprecipitation starter pack kit (#45-000-369, Cytiva, Marlborough, MA, USA), using the procedure according to the manufacturer. Protein samples were pretreated with agarose beads conjugated with protein A and rabbit IgG, followed by overnight immunoprecipitation with the beads conjugated with anti-EGFR or ALDOA antibodies. The beads were collected by centrifugation, washed three times with PBS, and resuspended for Western blotting. Western blotting was conducted using antibodies against EGFR and ALDOA (Cell Signaling).

Bone culture

A pair of femora were collected from C57BL/6 female mice (~10 weeks of age), and connective tissues around the bone were removed. The femora were cut in half at the mid-diaphysis, and a hole was generated at the other side with a 25-gauge needle. K7M2 OS cancer cells (2.5×10^5 cells) were resuspended in 10 μL of culture medium, and they were injected into the bone marrow cavity through the open end of the diaphysis. The bone samples were placed into a petri dish and cultured in 2 mL of DMEM with 10% FBS and 1% antibiotics at 37°C and 5% CO_2. Half of the culture media was replaced daily with fresh medium. After 2 weeks, the bone samples were used for Western blot analysis.

Osteoclast differentiation assay

The differentiation assay of RAW264.7 pre-osteoclasts was performed in a 12-well plate. During the 6-day incubation of pre-osteoclast cells in 40 ng/mL of RANKL, the CM was exchanged once on day 4. Adherent cells were fixed and stained with a tartrate-resistant acid phosphate (TRAP)-staining kit (Sigma), according to the manufacturer's instructions. TRAP-positive multinucleated cells (> 3 nuclei) were identified as mature osteoclasts.

Molecular docking analysis

To evaluate interactions between EGFR and ALDOA, as well as EGFR and P05, a ZDOCK program (ver. 2016, Discovery Studio, San Diego, CA, USA) was employed [44]. All possible binding poses were considered in the translational and rotational space between EGFR and ALDOA or P05, and each pose was evaluated by determining the energy-based ZDOCK scoring system [45]. Hydrogen-bonding interactions were predicted for the EGFR-ALDOA complex and EGFR-P05 complex.

Statistical analysis

For cell-based experiments, three or four independent experiments were conducted, and data were expressed as mean ± S.D. Statistical significance was evaluated using a one-way analysis of variance (ANOVA). Post hoc statistical comparisons with control groups were performed using Bonferroni correction with statistical significance at $P < 0.05$. The single and double asterisks in the figures indicate $P < 0.05$ and $P < 0.01$, respectively.

Results

Reduction in viability, and motility of OS cells by P02, P04, and P05

We first examined the ten anti-tumor peptide candidates (P01 to P10). They were selected from engineered MSC-derived CM that was enriched with anti-tumor proteins (Supplementary Table 1). The peptide candidates were derived from the trypsin-digested fragments of all proteins in the CM and their anticancer capability was evaluated using three OS cell lines (U2OS, TT2, and MG63). While the reduction of MTT-based cell viability in 2 days was observed with the peptides at 50 μg/ml except for peptide P06, the peptides (P02, P04, and P05) were the top three in the average reduction in the viability (Supplementary Table 2). Among these three peptides, P05 presented the most significant anti-tumor effects, particularly, on the MTT-based viability and scratch-based cell motility for TT2 OS cells (**Figure 1A**, **1B**). Importantly, these three peptides did not reduce the viability or motility of MSCs and hFOBs (**Figure 1C**, **1D**, Supplementary Figure 1A, 1B), indicating their cancer-selective inhibitory actions.

Reduction in proliferation, and invasion of OS cells by P05

The reduction in MTT viability was dose-dependent for P02, P04, and P05 (**Figure 2A**), and combinatorial use of these peptides presented an additive effect on the reduction in cell motility but not on the reduction in cell viability (**Figure 2B**, **2C**). Of note, P02 was derived from Rho GDP dissociation inhibitor alpha (ARHGDIA), while P04 and P05 were part of Aldolase A (ALDOA), a glycolytic enzyme. Besides viability and motility, P05 decreased the EdU-based proliferation and transwell invasion of TT2 OS cells (**Figure 3A**, **3B**). Furthermore, P05 decreased the scratch-based motility of U2OS and MG63 OS cells and the EdU-based proliferation of MG63 cells (Supplementary Figure 2A-C). Also, the application of P05 to TT2 OS cells downregulated oncoproteins such as p-Src, EGFR, and Snail, while it acted as a cytotoxic agent by elevating cleaved caspase 3, an

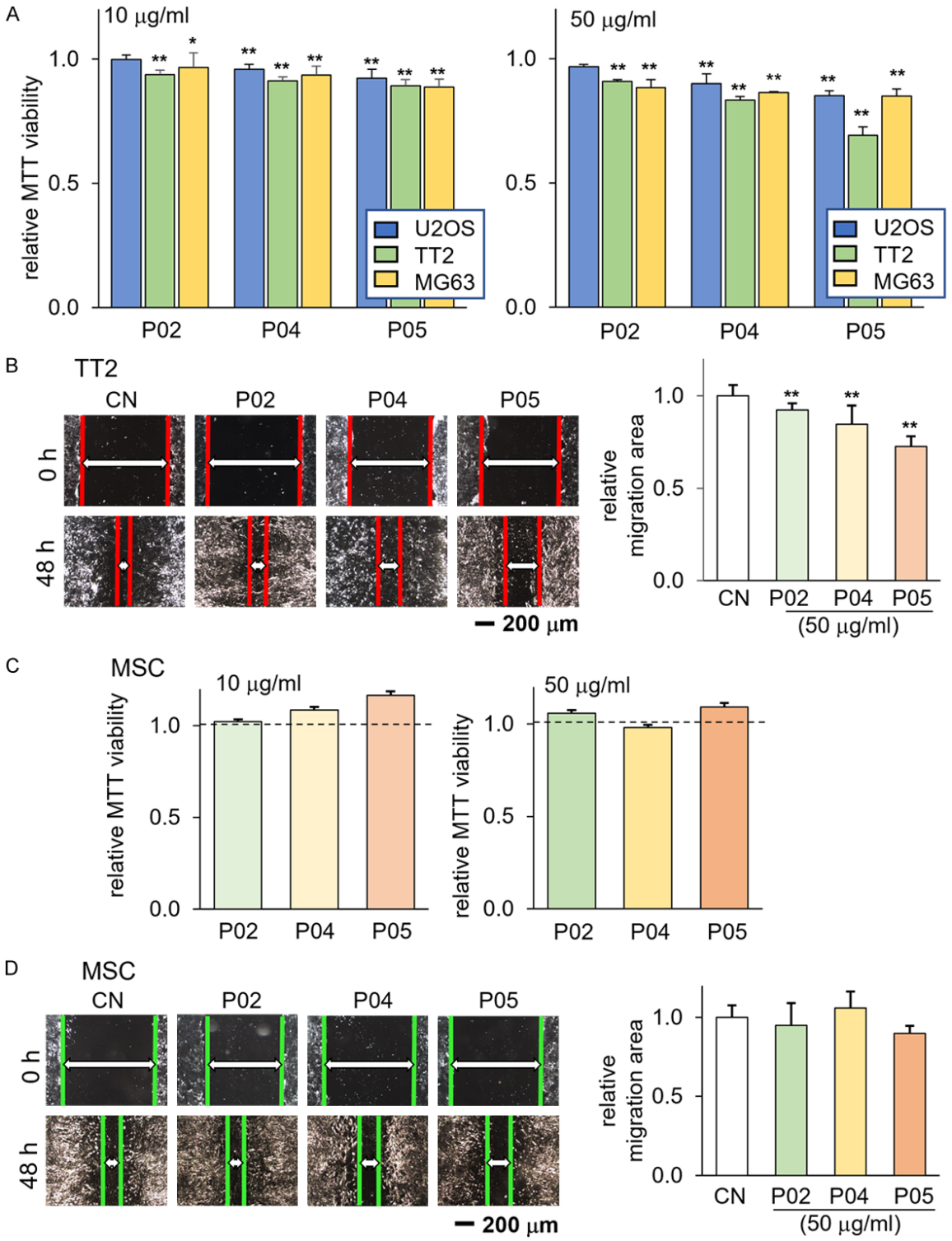

Figure 1. Anti-tumor action of P02, P04, and P05. MSC = mesenchymal stem cell, and CN = control. The single and double asterisks indicate $P < 0.05$ and 0.01, respectively. A, B. Reduction of MTT-based viability and scratch-based motility of U2OS, TT2, and MG63 osteosarcoma cells in response to 10 and 50 μg/ml P02, P04, and P05. C, D. No significant effects on MTT-based viability and scratch-based motility of MSCs in response to 10 and 50 μg/ml P02, P04, and P05.

apoptotic marker (**Figure 3C**). In MG63 OS cells, P05 also decreased the level of EGFR, p-Src, and Snail (Supplementary Figure 2D). Hereafter, we mainly examined the inhibitory action of

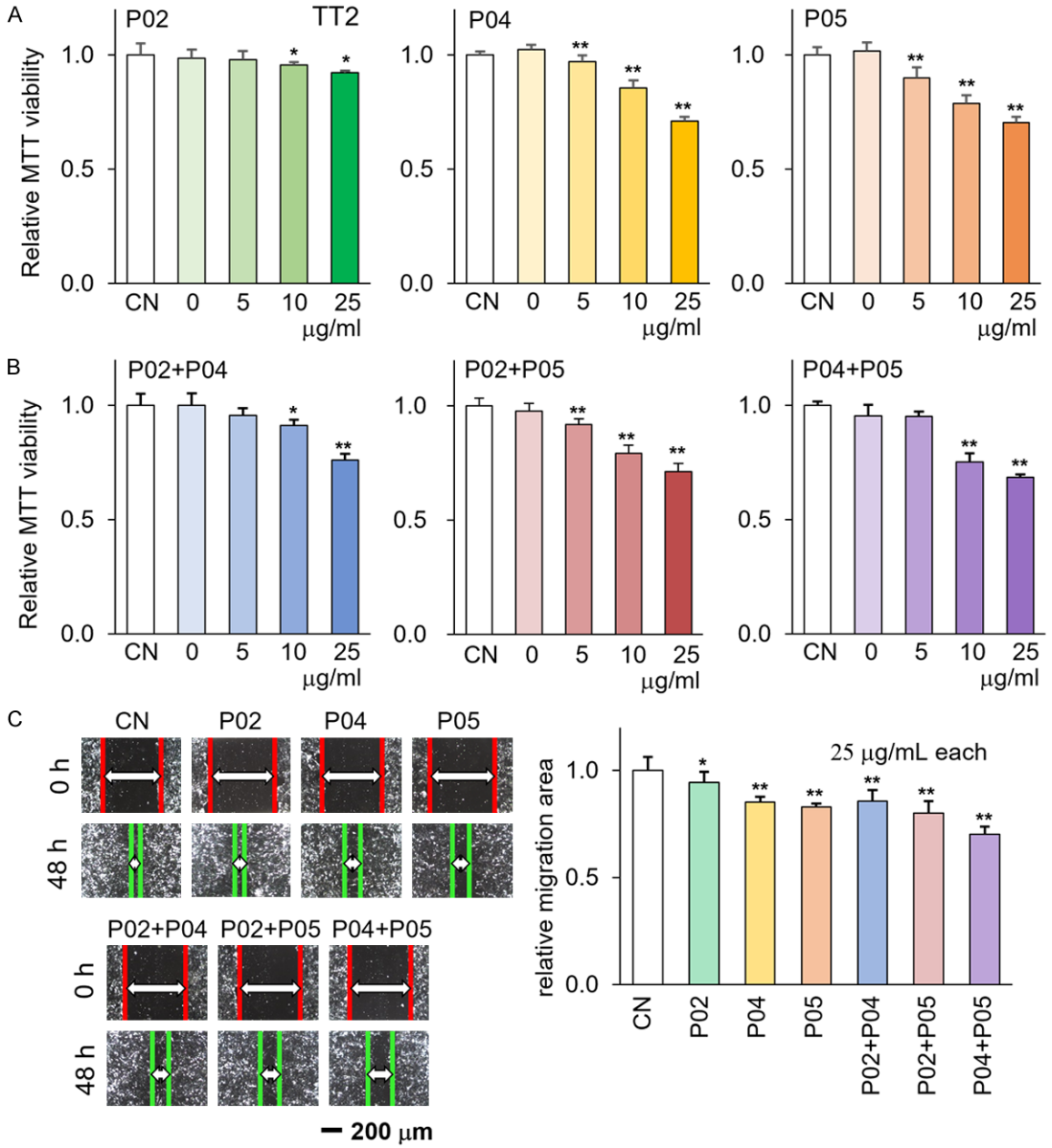

Figure 2. A Dose-dependent effects of P02, P04, and P05 on cell viability and motility. CN = control. The single and double asterisks indicate $P < 0.05$ and 0.01, respectively. A. Effects of P02, P04, and P05 on MTT-based viability of TT2 osteosarcoma cells. B, C. Combined effects of P02, P04, and P05 on MTT-based viability and scratch-based motility of TT2 osteosarcoma cells.

P05 because of its superior anti-tumor capabilities.

Additive anti-tumor effects with chemotherapeutic agents

We next examined the effects of the simultaneous application of P05 with three representative chemotherapeutic agents, such as Cisplatin, Doxorubicin, and Taxol. Cisplatin and Doxorubicin are two of the three agents in the standard-of-care chemotherapy for OS, while Taxol is the most well-known natural-source cancer drug. The result revealed that the application of P05 contributed to lowering the IC_{50} of the selected agents in MTT-based viability of TT2 OS cells (**Figure 3D**). With the application of P05 at 25 μg/ml, the IC_{50} value was lowered from 7.4 μM to 4.7 μM (Cisplatin), 2.6 μM to 0.9 μM (Doxorubicin), and 0.5 μM to 0.1 μM (Taxol).

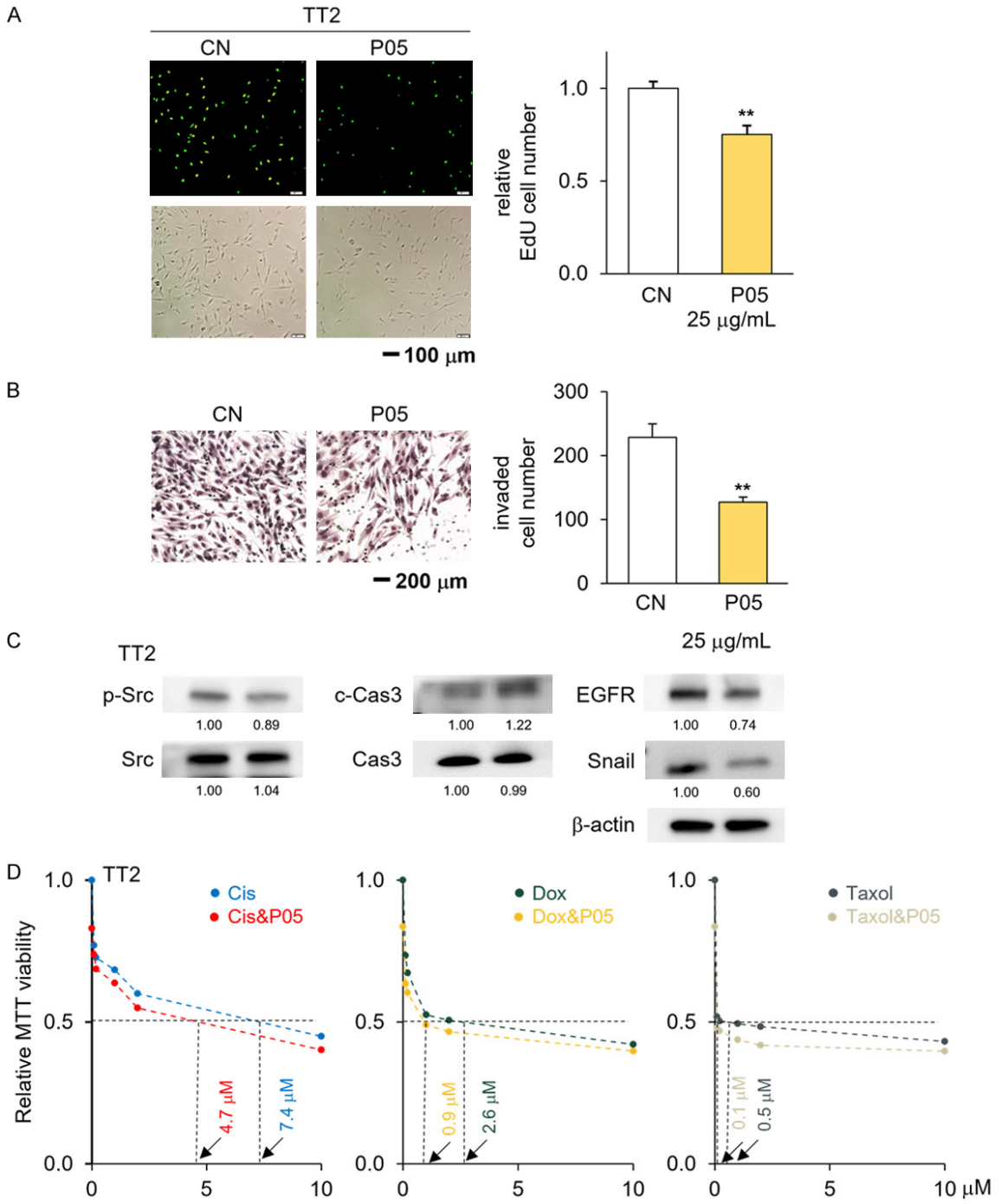

Figure 3. Effects of P05 on proliferation, invasion, and gene expression, and its combined effects with the selected chemotherapeutic agents. CN = control, Cis = Cisplatin, and Dox = Doxorubicin. The double asterisk indicates $P < 0.01$. A, B. Effects of 25 μg/ml P05 on proliferation and transwell invasion of TT2 osteosarcoma cells. C. Decrease in the levels of p-Src, EGFR, and Snail, and an increase in cleaved caspase 3 (c-Cas-3) in TT2 osteosarcoma cells by the application of 25 μg/ml P05. D. Additive anti-tumor effects of P05 with Cisplatin, Doxorubicin, or Taxol.

Anti-tumor effects on breast cancer cells by P02, P04, and P05

Besides the anti-OS actions, we observed that peptides P02, P04, and P05 suppressed the progression of breast cancer cells. The application of 25 μg/ml of P02, P04, and P05 significantly reduced MTT-based viability and scratch-based motility of MDA-MB-231 breast cancer cells (**Figure 4A**, **4B**).

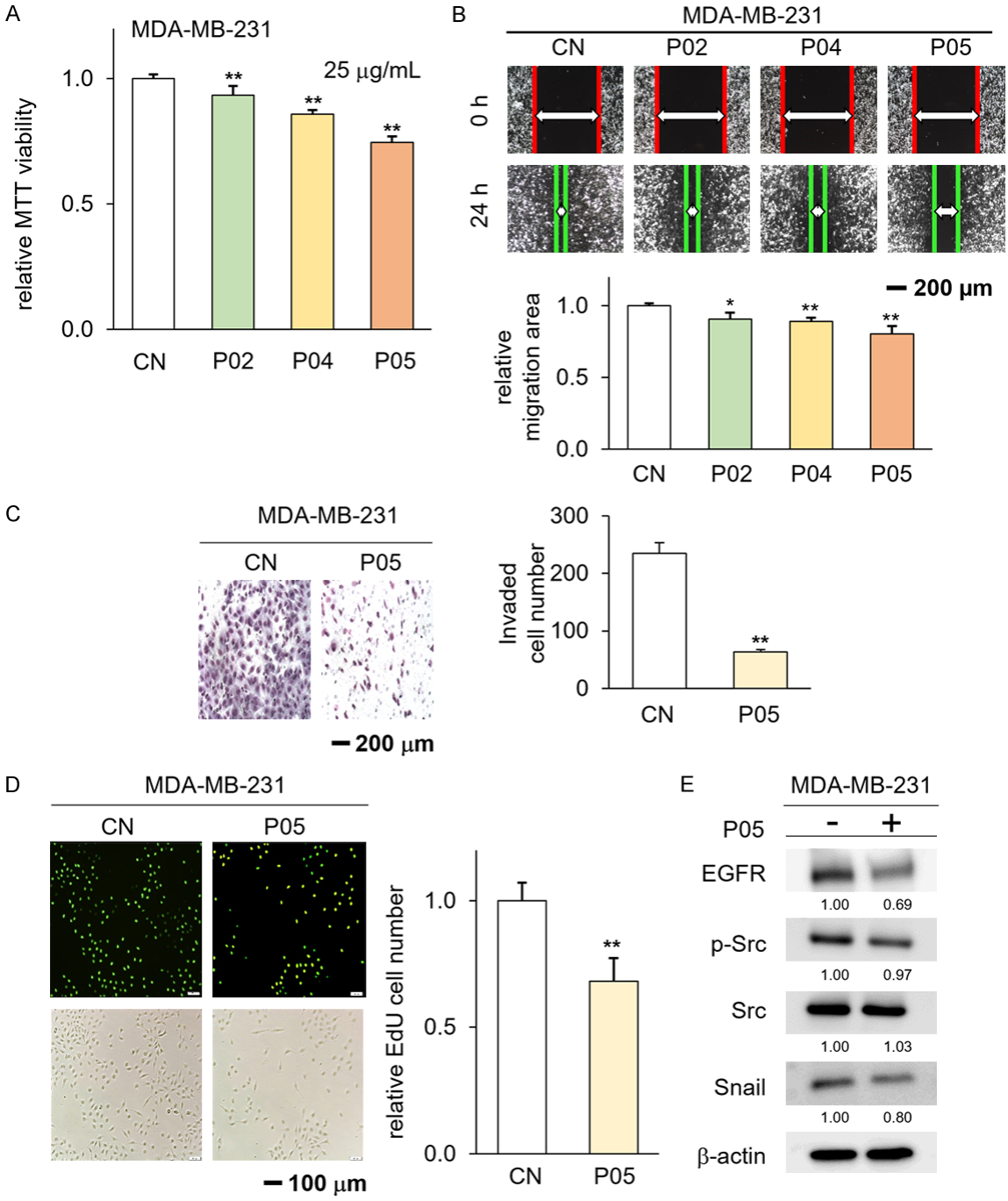

Figure 4. Anti-tumor effects of P02, P04, and P05 on MDA-MB-231 breast cancer cells. CN = control. The single and double asterisks indicate P < 0.05 and 0.01, respectively. A-D. Reduction in MTT-based viability, scratch-based motility, Transwell invasion, and EdU-based proliferation, respectively. E. Downregulation of oncoproteins such as EGFR, p-Src, and Snail by P05.

Furthermore, P05 significantly reduced transwell invasion and EdU-based proliferation of MDA-MB-231 cells (**Figure 4C**, **4D**). It also reduced the expression of EGFR, p-Src, and Snail (**Figure 4E**).

Generation of iTSCs by the overexpression of ALDOA in MSCs

Thus far, we show that P05, which is derived from ALDOA, can act as an ACP for OS and

breast cancer. We next evaluated the effect of ALDOA, a parental protein of P04 and P05, on OS cells and MSCs. As reported in our previous studies, most tumor-suppressing proteins, which were enriched in iTSC CM such as Moesin, Enolase 1, etc., presented a double-sided action as an oncoprotein intracellularly and a tumor suppressor extracellularly [46]. Here, we also observed the same site-dependent action of ALDOA. When ALDOA was overexpressed in TT2 and MG63 OS cells, it acted as an oncoprotein and stimulated the viability of OS cells (**Figure 5A**). However, when ALDOA was transfected into MSCs, ALDOA-overexpressing MSC-derived CM presented tumor-suppressing capabilities. This CM reduced viability, proliferation, motility, and invasion of TT2 OS cells (**Figure 5B-F**), as well as MG63 OS cells (Supplementary Figure 3).

Interaction between ALDOA and EGFR

In the IntAct molecular interaction database (EMBL-EBI), the interaction of ALDOA with EGFR was predicted (Supplementary Figure 4A). Consistently, a protein docking program, ZDOCK, predicted the potential binding of ALDOA with EGFR, including 22 possible interactions in the range of 1.9 to 3.7 Å (**Figure 6A**; Supplementary Table 3). Also, the possible binding of P05 with EGFR was shown with 10 putative hydrogen bondings at 1.9 to 3.6 Å (**Figure 6B**; Supplementary Table 4). An immunoprecipitation assay using a protein lysate from TT2 OS cells showed that ALDOA was co-immunoprecipitated with EGFR, and reciprocally EGFR was co-immunoprecipitated with ALDOA (**Figure 6C**, **6D**). Consistently, silencing of EGFR with its specific siRNA suppressed ALDOA-induced reduction in cell viability (**Figure 6E**). Collectively, ALDOA is a double-edged protein that acts as an oncoprotein intracellularly, as well as a tumor suppressor extracellularly. While the potential binding of P05 to EGFR was predicted, the interactions between ALDOA and EGFR (ZDOCK score of 27.78) were predicted stronger than those between P05 and EGFR (ZDOCK score of 15.76).

Inhibition of osteoclast maturation by P05

Bone-resorbing osteoclasts play a critical role in bone degradation in OS. Besides inhibiting the progression of OS cells, we examined the effects of P05 on the development of osteoclasts. The result showed that the differentiation of RANKL-stimulated osteoclasts was blocked and the number of multi-nucleated TRAP-positive osteoclasts (more than 3 nuclei) was significantly lowered by the application of P05 at 25 μg/ml (**Figure 7A**). By contrast, no significant change in the viability of MC3T3-E1 osteoblast cells was detected in response to P05, with a slight increase in type I collagen (COLI) and alkaline phosphatase (ALP) (Supplementary Figure 4B, 4C).

Reduction of oncoproteins by P05 in the ex vivo bone culture

Given the anticancer role of P05 in OS cells, we lastly examined its tumor-suppressing effect using an ex vivo bone culture. K7M2 OS cell-inoculated femora were cultured in the presence and absence of 25 μg/mL P05 for 2 weeks, and the expression of oncoproteins was evaluated. The result revealed that the administration of P05 significantly reduced the levels of EGFR, macrophage colony-stimulating factor (M-CSF), osteopontin (OPN), interleukin 1 beta (IL-1β), interleukin 6 (IL-6), and phosphorylated Src (**Figure 7B**).

Discussion

This study presented that peptide P05 acted as an effective ACP for OS cells as well as breast cancer cells. P05 is derived from a glycolytic enzyme, ALDOA, having an amino acid sequence of ADDGRPFPQVIK (1,342 Da) with an isoelectric point of 7.0. The application of P05 inhibited the viability, proliferation, motility, and invasion of human OS cell lines. It also downregulated the expression of oncogenic proteins such as Src, Snail, and EGFR and induced apoptosis by elevating the level of cleaved caspase 3. P04 was also derived from ALDOA and acted as another ACP (2,107 Da for IGEHTPSALAIMENANVLAR) with an isoelectric point of 5.3. Most ACPs are positively charged since cancer cells have in general negative surface charges because of the glycolysis-driven secretion of lactic acid. Interestingly, unlike most ACPs, the net charge of P04 and P05 is negative at a neutral pH. The result indicates that the selective interaction of P04 and P05 with OS cells is not mediated by non-specific electrostatic force.

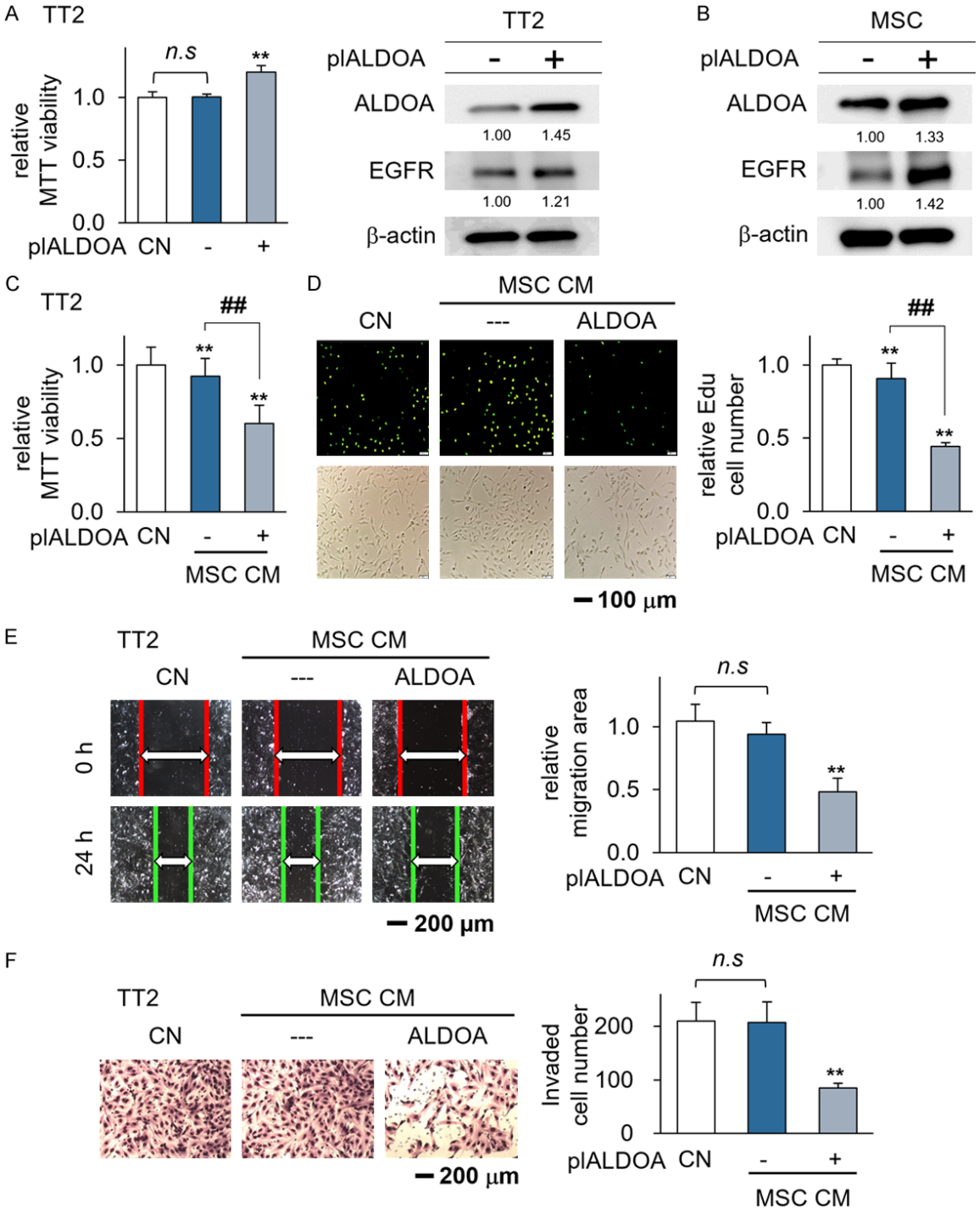

Figure 5. Double-edged role of ALDOA to osteosarcoma and MSCs. CN = control, pl = plasmid transfection, MSC = mesenchymal stem cell, and CM = conditioned medium. The double asterisk indicates $P < 0.01$. A. Increase in MTT-based viability and the level of EGFR by overexpressing ALDOA in TT2 osteosarcoma cells. B. Overexpression of ALDOA in MSCs and the elevation of EGFR. C-F. Reduction in MTT-based viability, EdU-based proliferation, scratch-based motility, and transwell invasion, respectively, by ALDOA-overexpressing MSC-derived conditioned medium.

We observed a double-sided role of ALDOA, depending on its acting site in the intracellular and extracellular domains. Similar to atypical tumor-suppressing proteins, such as Moesin and Enolase 1, its overexpression in tumor cells elevated their MTT-based viability.

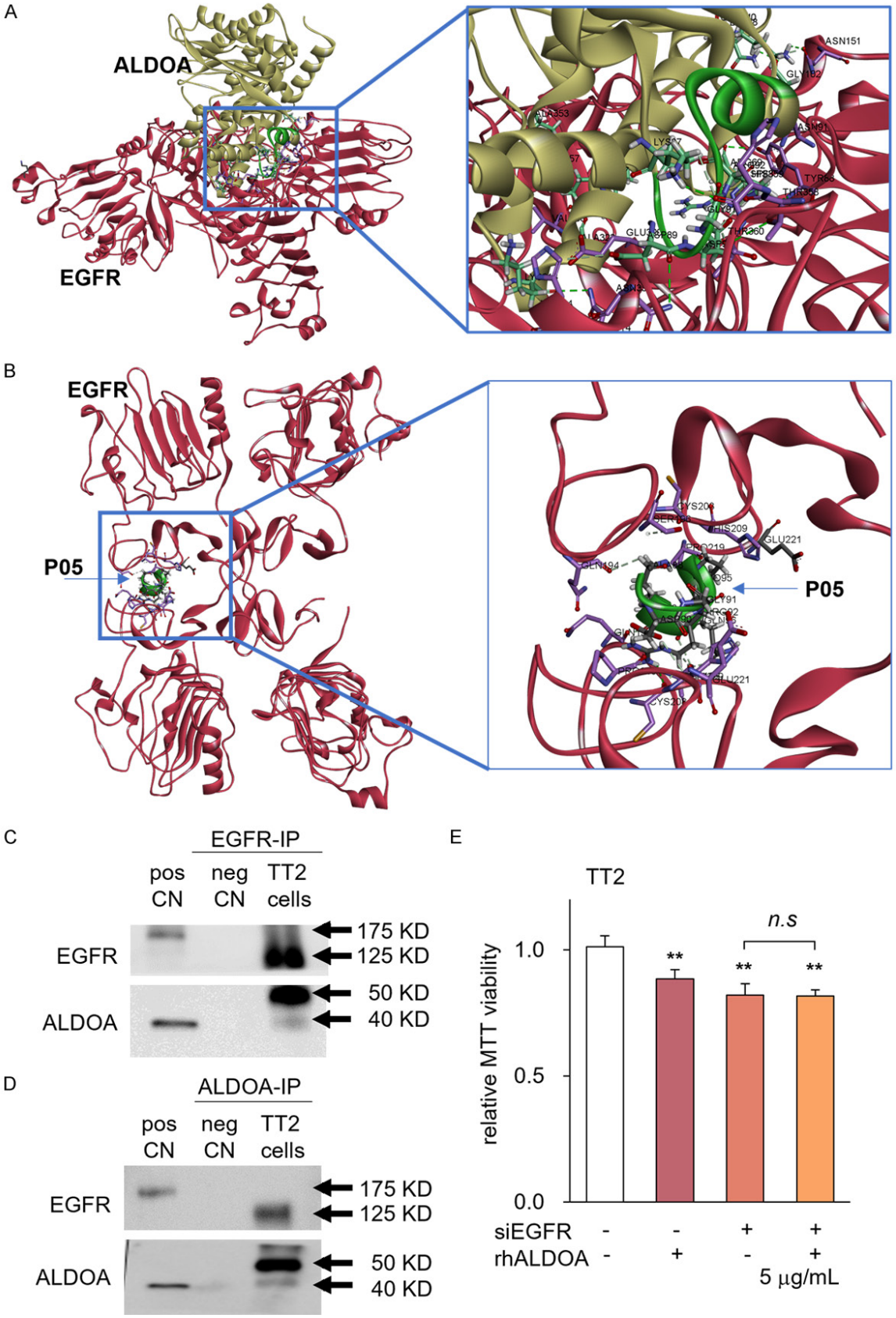

Figure 6. Possible involvement of EGFR in the action of ALDOA and P05. CN = control. The double asterisk indicates $P < 0.01$. A, B. Predicted interactions of ALDOA-EGFR and P05-EGFR. C, D. Reciprocal immunoprecipitation of EGFR and ALDOA using TT2 derived cell lysates. E. Suppression of ALDOA-driven reduction in MTT-based viability of TT2 OS cells by silencing EGFR.

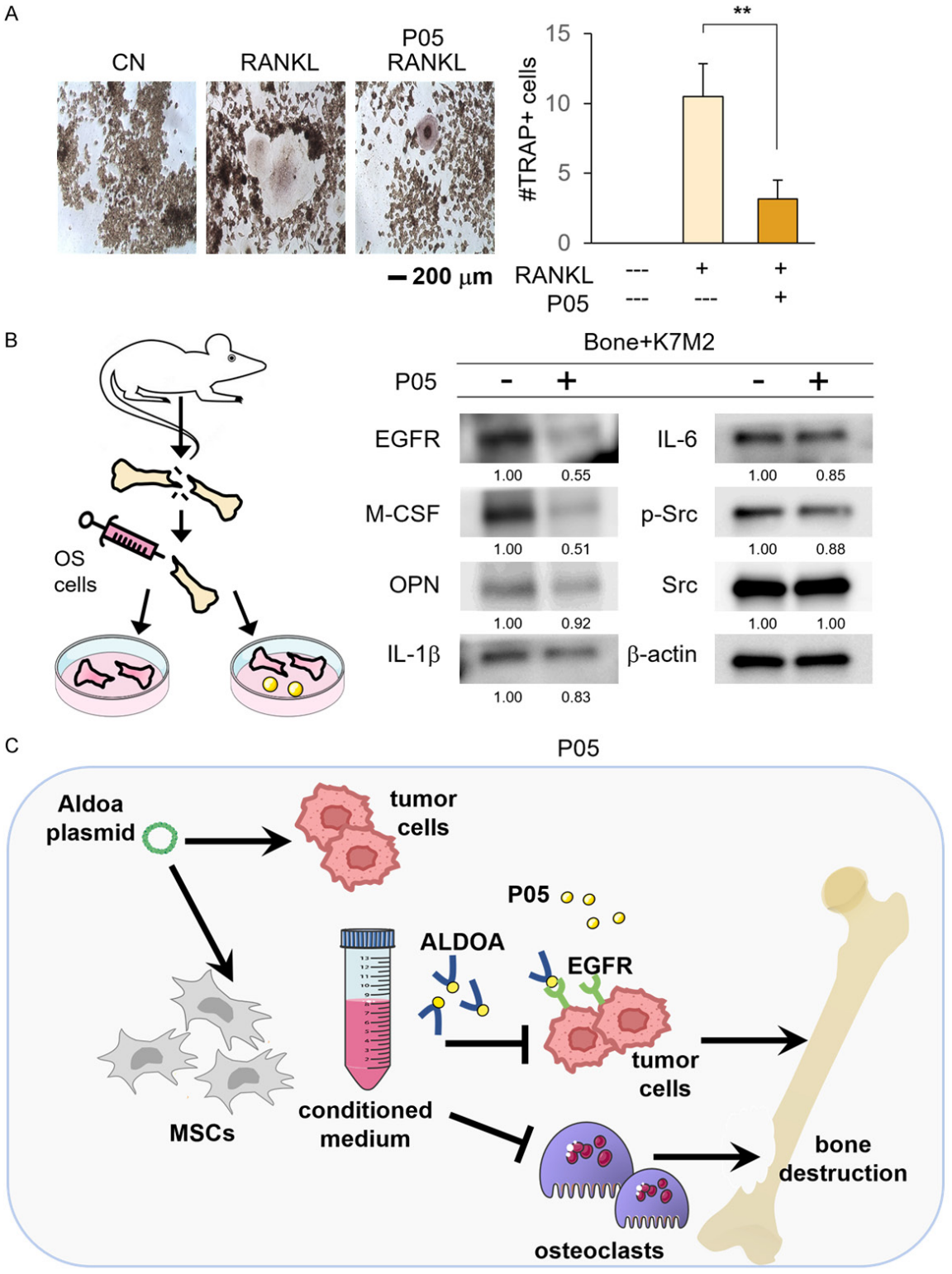

Figure 7. P05's protective effects on bone and the proposed mechanism of P05's action. CN = control. The double asterisk indicates $P < 0.01$. A. Reduction in multi-nucleated RANKL-stimulated osteoclasts in response to P05. B. Reduction in EGFR, M-CSF, OPN, IL-1β, IL6, and p-Src by the administration of 25 μg/mL of P05 in the *ex vivo* bone culture. C. Proposed mechanism of the anti-tumor action of P05.

However, ALDOA-overexpressing MSCs generated tumor-suppressing CM, and extracellular ALDOA acted as a tumor suppressor. The protein docking analysis and immunoprecipitation assay supported the interaction of ALDOA with EGFR. The overexpression of EGFR promoted the growth and motility of OS cells, while its deletion suppressed the proliferation, migration, and invasion of OS cells *in vitro* and tumor formation *in vivo* [47]. The levels of phospho-Akt and phospho-ERK were decreased by EGFR knockdown but increased as a result of EGFR overexpression, supporting a possible involvement of PI3K/Akt and ERK pathways in the effects of EGFR on OS cells [48].

Deep learning-based analyses present a list of selection criteria for predicting effective ACPs [49, 50]. The criteria include (a) enrichment of G, A, L, F, W, and K residues, (b) high frequency of the positively charged residue K and low frequency of the negatively charged residues of D and E, (c) a net positive charge with a high isoelectric point, and (d) frequent appearance of specific pairing. The net charge at pH 7 was 0 (P05) and -0.91 (P04). According to one of the prediction software iDACP [51], P04 and P05 were predicted as non-ACPs with a score of 0.039 and 0.074, respectively, in which the score range was 0 (most likely non-ACP) to 1 (most likely ACP). The non-ACP prediction by iDACP indicates the difficulty in predicting effective ACPs.

The proposed mechanism of P05's action is illustrated in **Figure 7C**. The overexpression of ALDOA in OS cells promoted their viability, but ALDOA-overexpressing MSC CM, as well as extracellular ALDOA, suppressed the progression of OS cells. ALDOA-derived P05 also inhibited the proliferation, migration, and invasion of OS cells. The additive effect of P05 and chemotherapeutic agents is an advantage for clinical applications. Patients do not have to eliminate the current standard-of-care treatment. The simultaneous application of P05 significantly reduced IC_{50} of Cisplatin, Doxorubicin, and Taxol. The additive therapeutic action would reduce the toxic effects of the chemotherapeutic agents by reducing their dosage. Besides the suppression of OS progression, P05 was effective in blocking the differentiation of bone-resorbing osteoclasts.

We recognize that there are limitations to the current study. The stability, specificity, and side effects of P05 should be evaluated using preclinical models. While the molecular docking analysis predicted a possible interaction of P05 with EGFR, an experimental evaluation is necessary to determine whether the anticancer action of P05 is mediated with EGFR. For the clinical application to OS, P05's bone-targeted delivery is expected to enhance its efficacy and preclinical studies should be conducted.

Conclusions

This study demonstrated that P05 is a candidate for anti-OS APC that suppressed the viability, motility, and invasion capability of three OS cell lines. P05 can be applied with existing chemotherapeutic agents, and it significantly reduced the IC_{50} of each of the three tested agents. The anticancer action of P05 is not based on nonspecific electrostatic interactions with negatively charged cancer cells. Further studies are recommended to determine its anti-cancer mechanism, including possible interaction with EGFR.

Acknowledgements

The authors appreciated a web-based tool, iDACP, for the prediction of anticancer peptides. This research was funded by the National Institutes of Health, P30CA082709 (KEP); and the National Natural Science Foundation of China, 81971326 (BYL).

Disclosure of conflict of interest

None.

Address correspondence to: Hiroki Yokota, Department of Biomedical Engineering, Indiana University Purdue University Indianapolis, Indianapolis, IN 46202, USA. E-mail: hyokota@iupui.edu; Bai-Yan Li, Department of Pharmacology, School of Pharmacy, Harbin Medical University, Harbin 150081, Heilongjiang, China. E-mail: liby@ems.hrbmu.edu.cn

References

[1] Harrison DJ, Geller DS, Gill JD, Lewis VO and Gorlick R. Current and future therapeutic approaches for osteosarcoma. Expert Rev Anticancer Ther 2018; 18: 39-50.

[2] Odri GA, Tchicaya-Bouanga J, Yoon DJY and Modrowski D. Metastatic progression of osteosarcomas: a review of current knowledge of environmental versus oncogenic drivers. Cancers (Basel) 2022; 14: 360.

[3] Kager L, Tamamyan G and Bielack S. Novel insights and therapeutic interventions for pediatric osteosarcoma. Future Oncol 2017; 13: 357-368.
[4] Thai VL, Griffin KH, Thorpe SW, Randall RL and Leach JK. Tissue engineered platforms for studying primary and metastatic neoplasm behavior in bone. J Biomech 2021; 115: 110189.
[5] Smrke A, Anderson PM, Gulia A, Gennatas S, Huang PH and Jones RL. Future directions in the treatment of osteosarcoma. Cells 2021; 10: 172.
[6] Chung DY, Kang DH, Kim JW, Ha JS, Kim DK and Cho KS. Comparison of oncologic outcomes of dose-dense methotrexate, vinblastine, doxorubicin, and cisplatin (ddMVAC) with gemcitabine and cisplatin (GC) as neoadjuvant chemotherapy for muscle-invasive bladder cancer: systematic review and meta-analysis. Cancers (Basel) 2021; 13: 2770.
[7] Gordon N, Felix K and Daw NC. Aerosolized chemotherapy for osteosarcoma. Adv Exp Med Biol 2020; 1257: 67-73.
[8] Jafari F, Javdansirat S, Sanaie S, Naseri A, Shamekh A, Rostamzadeh D and Dolati S. Osteosarcoma: a comprehensive review of management and treatment strategies. Ann Diagn Pathol 2020; 49: 151654.
[9] Ghaly G, Tallima H, Dabbish E, Badr ElDin N, Abd El-Rahman MK, Ibrahim MAA and Shoeib T. Anti-cancer peptides: status and future prospects. Molecules 2023; 28: 1148.
[10] Tornesello AL, Borrelli A, Buonaguro L, Buonaguro FM and Tornesello ML. Antimicrobial peptides as anticancer agents: functional properties and biological activities. Molecules 2020; 25: 2850.
[11] Hilchie AL, Hoskin DW and Power Coombs MR. Anticancer activities of natural and synthetic peptides. Adv Exp Med Biol 2019; 1117: 131-147.
[12] Kordi M, Borzouyi Z, Chitsaz S, Asmaei MH, Salami R and Tabarzad M. Antimicrobial peptides with anticancer activity: today status, trends and their computational design. Arch Biochem Biophys 2023; 733: 109484.
[13] Xie M, Liu D and Yang Y. Anti-cancer peptides: classification, mechanism of action, reconstruction and modification. Open Biol 2020; 10: 200004.
[14] Bose D, Roy L and Chatterjee S. Peptide therapeutics in the management of metastatic cancers. RSC Adv 2022; 12: 21353-21373.
[15] Marqus S, Pirogova E and Piva TJ. Evaluation of the use of therapeutic peptides for cancer treatment. J Biomed Sci 2017; 24: 21.
[16] Palazzi L, Pasquato A, Vicario M, Roulin A, Polverino de Laureto P and Cendron L. C-terminal tails mimicking bioactive intermediates cause different plasma degradation patterns and kinetics in neuropeptides γ-MSH, α-MSH, and neurotensin. J Pept Sci 2020; 26: e3279.
[17] Garai S, Thomas J, Dey P and Das D. LGBM-ACp: an ensemble model for anticancer peptide prediction and in silico screening with potential drug targets. Mol Divers 2023; [Epub ahead of print].
[18] Gupta KK, Sharma KK, Chandra H, Panwar H, Bhardwaj N, Altwaijry NA, Alsfouk AA, Dlamini Z, Afzal O, Altamimi ASA, Khan S and Mishra AP. The integrative bioinformatics approaches to predict the xanthohumol as anti-breast cancer molecule: targeting cancer cells signaling PI3K and AKT kinase pathway. Front Oncol 2022; 12: 950835.
[19] Jawarkar RD, Sharma P, Jain N, Gandhi A, Mukerjee N, Al-Mutairi AA, Zaki MEA, Al-Hussain SA, Samad A, Masand VH, Ghosh A and Bakal RL. QSAR, molecular docking, MD simulation and MMGBSA calculations approaches to recognize concealed pharmacophoric features requisite for the optimization of ALK tyrosine kinase inhibitors as anticancer leads. Molecules 2022; 27: 4951.
[20] Yadav M and Eswari JS. Opportunistic challenges of computer-aided drug discovery of lipopeptides: new insights for large molecule therapeutics. Avicenna J Med Biotechnol 2023; 15: 3-13.
[21] Li K, Huo Q, Li BY and Yokota H. The double-edged proteins in cancer proteomes and the generation of induced tumor-suppressing cells (iTSCs). Proteomes 2023; 11: 5.
[22] Sun X, Li KX, Figueiredo ML, Lin CC, Li BY and Yokota H. Generation of the chondroprotective proteomes by activating PI3K and TNFα signaling. Cancers (Basel) 2022; 14: 3039.
[23] Liu S, Wu D, Sun X, Fan Y, Zha R, Jalali A, Feng Y, Li K, Sano T, Vike N, Li F, Rispoli J, Sudo A, Liu J, Robling A, Nakshatri H, Li BY and Yokota H. Overexpression of Lrp5 enhanced the anti-breast cancer effects of osteocytes in bone. Bone Res 2021; 9: 32.
[24] Sun X, Li K, Zha R, Liu S, Fan Y, Wu D, Hase M, Aryal UK, Lin CC, Li BY and Yokota H. Preventing tumor progression to the bone by induced tumor-suppressing MSCs. Theranostics 2021; 11: 5143-5159.
[25] Sano T, Sun X, Feng Y, Liu S, Hase M, Fan Y, Zha R, Wu D, Aryal UK, Li BY, Sudo A and Yokota H. Inhibition of the growth of breast cancer-associated brain tumors by the osteocyte-derived conditioned medium. Cancers (Basel) 2021; 13: 1061.
[26] Feng Y, Liu S, Zha R, Sun X, Li K, Robling A, Li B and Yokota H. Mechanical loading-driven tumor suppression is mediated by Lrp5-depen-

dent and independent mechanisms. Cancers (Basel) 2021; 13: 267.
[27] Sun X, Li K, Hase M, Zha R, Feng Y, Li BY and Yokota H. Suppression of breast cancer-associated bone loss with osteoblast proteomes via Hsp90ab1/moesin-mediated inhibition of TGFβ/FN1/CD44 signaling. Theranostics 2022; 12: 929-943.
[28] Banito A and Gil J. Induced pluripotent stem cells and senescence: learning the biology to improve the technology. EMBO Rep 2010; 11: 353-359.
[29] Bonaventura G, Iemmolo R, Attaguile GA, La Cognata V, Pistone BS, Raudino G, D'Agata V, Cantarella G, Barcellona ML and Cavallaro S. iPSCs: a preclinical drug research tool for neurological disorders. Int J Mol Sci 2021; 22: 4596.
[30] Gähwiler EKN, Motta SE, Martin M, Nugraha B, Hoerstrup SP and Emmert MY. Human iPSCs and genome editing technologies for precision cardiovascular tissue engineering. Front Cell Dev Biol 2021; 9: 639699.
[31] Takahashi K, Tanabe K, Ohnuki M, Narita M, Ichisaka T, Tomoda K and Yamanaka S. Induction of pluripotent stem cells from adult human fibroblasts by defined factors. Cell 2007; 131: 861-872.
[32] Yu J, Vodyanik MA, Smuga-Otto K, Antosiewicz-Bourget J, Frane JL, Tian S, Nie J, Jonsdottir GA, Ruotti V, Stewart R, Slukvin II and Thomson JA. Induced pluripotent stem cell lines derived from human somatic cells. Science 2007; 318: 1917-1920.
[33] Kuilman T, Michaloglou C, Vredeveld LC, Douma S, van Doorn R, Desmet CJ, Aarden LA, Mooi WJ and Peeper DS. Oncogene-induced senescence relayed by an interleukin-dependent inflammatory network. Cell 2008; 133: 1019-1031.
[34] Tochio T, Tanaka H, Nakata S and Hosoya H. Fructose-1,6-bisphosphate aldolase A is involved in HaCaT cell migration by inducing lamellipodia formation. J Dermatol Sci 2010; 58: 123-129.
[35] Gizak A, Wiśniewski J, Heron P, Mamczur P, Sygusch J and Rakus D. Targeting a moonlighting function of aldolase induces apoptosis in cancer cells. Cell Death Dis 2019; 10: 712.
[36] Wiese EK, Hitosugi S, Loa ST, Sreedhar A, Andres-Beck LG, Kurmi K, Pang YP, Karnitz LM, Gonsalves WI and Hitosugi T. Enzymatic activation of pyruvate kinase increases cytosolic oxaloacetate to inhibit the Warburg effect. Nat Metab 2021; 3: 954-968.
[37] Liu S, Sun X, Li K, Zha R, Feng Y, Sano T, Dong C, Liu Y, Aryal UK, Sudo A, Li BY and Yokota H. Generation of the tumor-suppressive secretome from tumor cells. Theranostics 2021; 11: 8517-8534.
[38] Rossi M, Cappadone C, Picone G, Bisi A, Farruggia G, Belluti F, Blasi P, Gobbi S and Malucelli E. Natural-like chalcones with antitumor activity on human MG63 osteosarcoma cells. Molecules 2022; 27: 3751.
[39] Kasiram MZ, Hapidin H, Abdullah H, Hashim NM, Azlina A and Sulong S. Tannic acid enhances cisplatin effect on cell proliferation and apoptosis of human osteosarcoma cell line (U2OS). Pharmacol Rep 2022; 74: 175-188.
[40] Li K, Huo Q, Dimmitt NH, Qu G, Bao J, Pandya PH, Saadatzadeh MR, Bijangi-Vishehsaraei K, Kacena MA, Pollok KE, Lin CC, Li BY and Yokota H. Osteosarcoma-enriched transcripts paradoxically generate osteosarcoma-suppressing extracellular proteins. Elife 2023; 12: e83768.
[41] Christie JD, Appel N, Zhang L, Lowe K, Kilbourne J, Daggett-Vondras J, Elliott N, Lucas AR, Blattman JN, Rahman MM and McFadden G. Systemic delivery of mLIGHT-armed myxoma virus is therapeutic for later-stage syngeneic murine lung metastatic osteosarcoma. Cancers (Basel) 2022; 14: 337.
[42] Miura K. Imaging technologies for the detection of multiple stains in proteomics. Proteomics 2003; 3: 1097-1108.
[43] Elebro J, Heby M, Warfvinge CF, Nodin B, Eberhard J and Jirström K. Expression and prognostic significance of human epidermal growth factor receptors 1, 2 and 3 in periampullary adenocarcinoma. PLoS One 2016; 11: e0153533.
[44] Aramyan S, McGregor K, Sandeep S and Haczku A. SP-A binding to the SARS-CoV-2 spike protein using hybrid quantum and classical in silico modeling and molecular pruning by quantum approximate optimization algorithm (QAOA) based maxcut with ZDOCK. Front Immunol 2022; 13: 945317.
[45] Barradas-Bautista D, Cao Z, Vangone A, Oliva R and Cavallo L. A random forest classifier for protein-protein docking models. Bioinform Adv 2021; 2: vbab042.
[46] Sun X, Li K, Li BY and Yokota H. Wnt signaling: a double-edged sword in protecting bone from cancer. J Bone Miner Metab 2023; 41: 365-370.
[47] Tateyama N, Suzuki H, Ohishi T, Asano T, Tanaka T, Mizuno T, Yoshikawa T, Kawada M, Kaneko MK and Kato Y. Antitumor activity of an anti-EGFR/HER2 bispecific antibody in a mouse xenograft model of canine osteosarcoma. Pharmaceutics 2022; 14: 2494.
[48] Wang S, Wei H, Huang Z, Wang X, Shen R, Wu Z and Lin J. Epidermal growth factor receptor promotes tumor progression and contributes

to gemcitabine resistance in osteosarcoma. Acta Biochim Biophys Sin (Shanghai) 2021; 53: 317-324.

[49] Huang KY, Tseng YJ, Kao HJ, Chen CH, Yang HH and Weng SL. Identification of subtypes of anticancer peptides based on sequential features and physicochemical properties. Sci Rep 2021; 11: 13594.

[50] Thi Phan L, Woo Park H, Pitti T, Madhavan T, Jeon YJ and Manavalan B. MLACP 2.0: an updated machine learning tool for anticancer peptide prediction. Comput Struct Biotechnol J 2022; 20: 4473-4480.

[51] Andersson M, Leggett RW, Eckerman K, Almén A and Mattsson S. IDAC-Bio, a software for internal dosimetry based on the new ICRP biokinetic models and specific absorbed fractions. Health Phys 2022; 123: 165-172.

Supplementary Table 1. Anti-cancer peptide candidates

id	sequence	gene	MW (Da)	Isoelectric point (PH)	net chart at pH 7.0
P01	SETAPAAPAAPAPAEK	Histone H1.4 (H1-4)	1478.6	4.30	-1.00
P02	AEEYEFLTPMEEAPK	Rho GDP Dissociation Inhibitor Alpha (ARHGDIA)	1784.0	3.67	-3.99
P03	HVFGESDELIGQK	Triosephosphate Isomerase (TPI)	1458.3	4.43	-1.91
P04	IGEHTPSALAIMENANVLAR	ALDOA (Aldolase A)	2107.4	5.30	-0.91
P05	ADDGRPFPQVIK	ALDOA (Aldolase A)	1342.5	7.00	0.00
P06	GAGTGGLGLAVEGPSEAK	FLNA (Filamin A)	1570.7	4.27	-1.00
P07	VEPGLGADNSVVR	FLNA (Filamin A)	1312.4	4.07	-1.00
P08	NSNLVGAAHEELQQSR	Lamin A/C (LMNA)	1752.9	5.30	-0.91
P09	AAGTLYTYPENWR	Eukaryotic Translation Elongation Factor 1 Gamma (Eef1G)	1541.7	7.00	0.00
P10	FAAATGATPIAGR	40S ribosomal protein	1203.4	11.05	1.00

Supplementary Table 2. MTT-based relative viability of 3 osteosarcoma cell lines

	Application of 50 μg/ml of P01 to P10									
	P01	P02	P03	P04	P05	P06	P07	P08	P09	P10
U2OS	1.13	0.93	0.98	0.83	0.98	1.17	0.96	1.06	1.07	1.01
TT2	0.79	0.91	0.80	0.86	0.84	0.99	0.95	0.83	0.85	0.87
MG63	0.84	0.88	1.04	0.86	0.85	0.92	0.96	0.92	0.85	1.08
mean	0.92	0.91	0.94	0.85	0.89	1.02	0.96	0.94	0.93	0.99

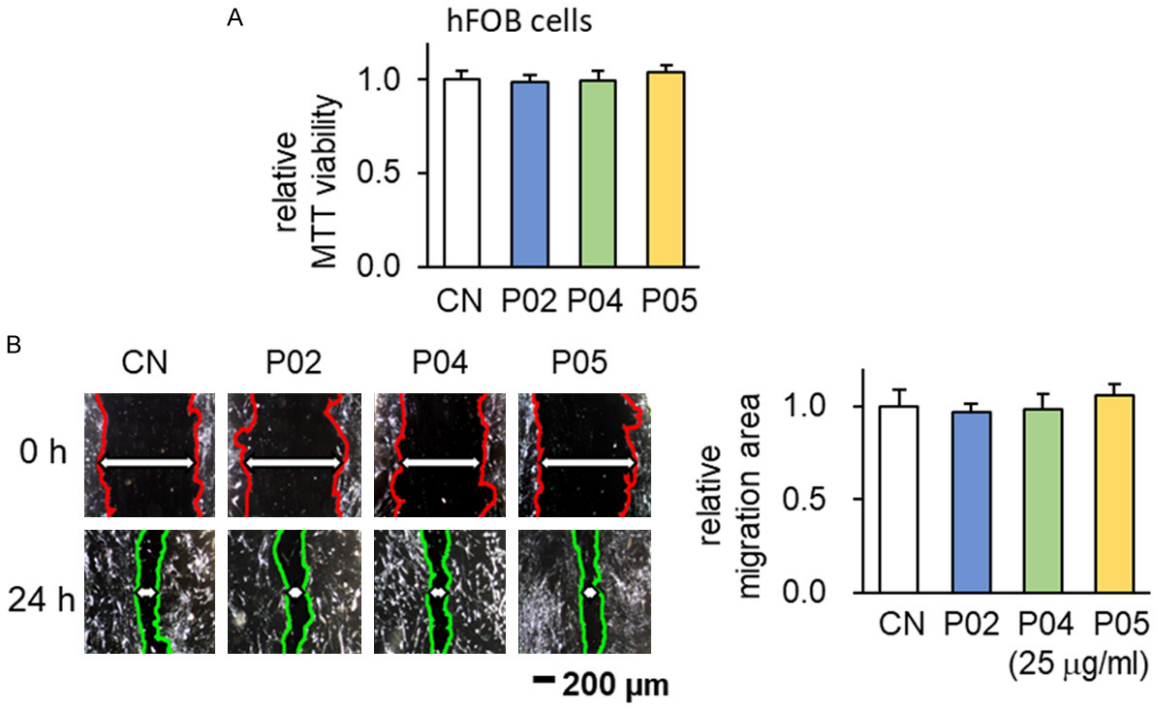

Supplementary Figure 1. Effect of P02, P04, and P05 on hFOB cells. CN = control. A, B. No significant change in the MTT-based viability and scratch-based motility, respectively, in response to the administration of 25 μg/ml of P02, P04, or P05.

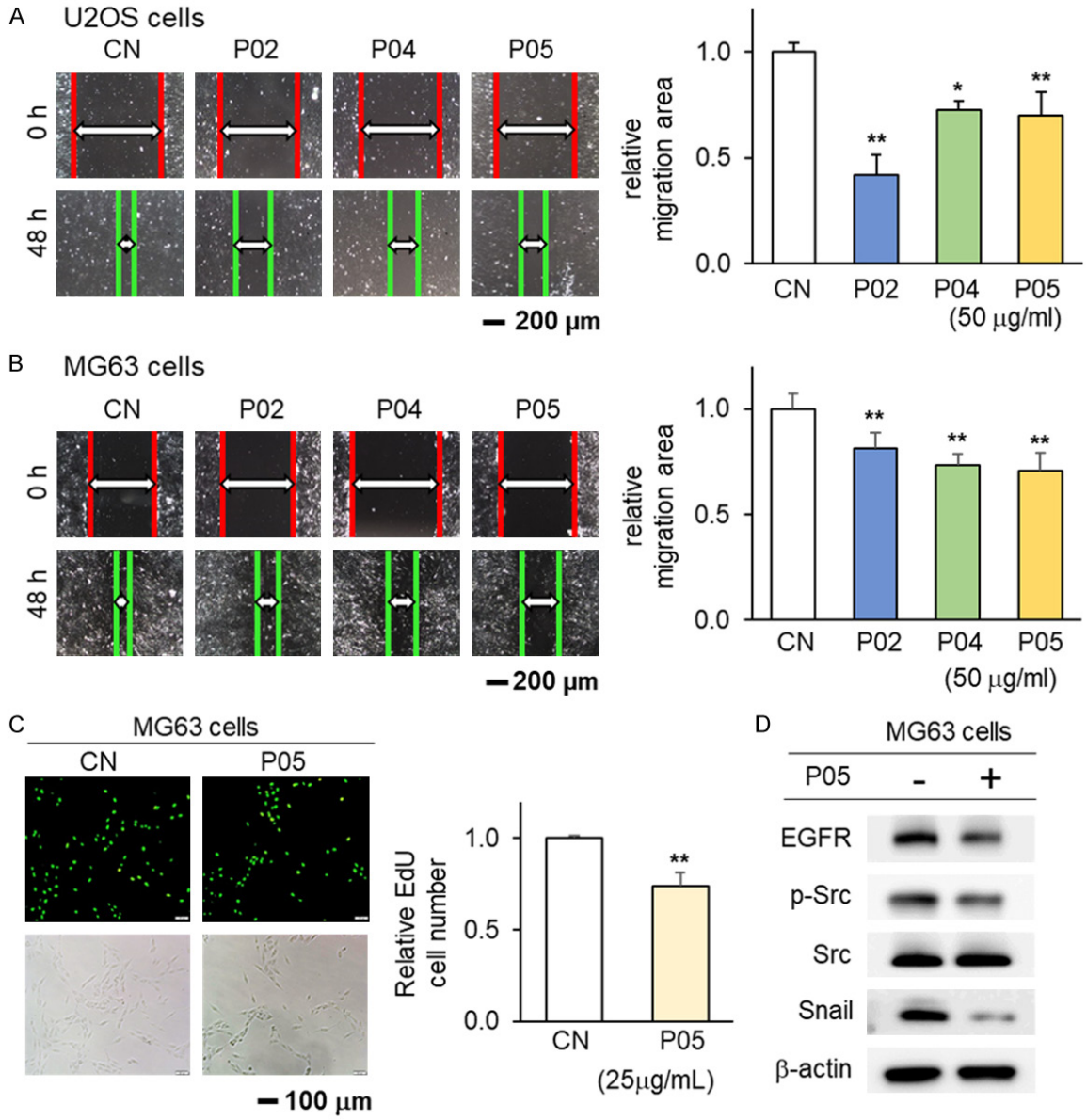

Supplementary Figure 2. Anti-tumor action of P02, P04, and P05 to U2OS and MG63 osteosarcoma cells. CN = control. The single and double asterisks indicate $P < 0.05$ and 0.01, respectively. A, B. Reduction in scratch-based motility of U2OS and MG63 osteosarcoma cells, respectively, by the application of 50 μg/ml of P02, P04, and P05. C. Reduction in EdU-based proliferation of MG63 cells by 25 μg/ml of P05. D. Downregulation of EGFR, p-Src, and Snail in MG63 cells by 25 μg/ml of P05.

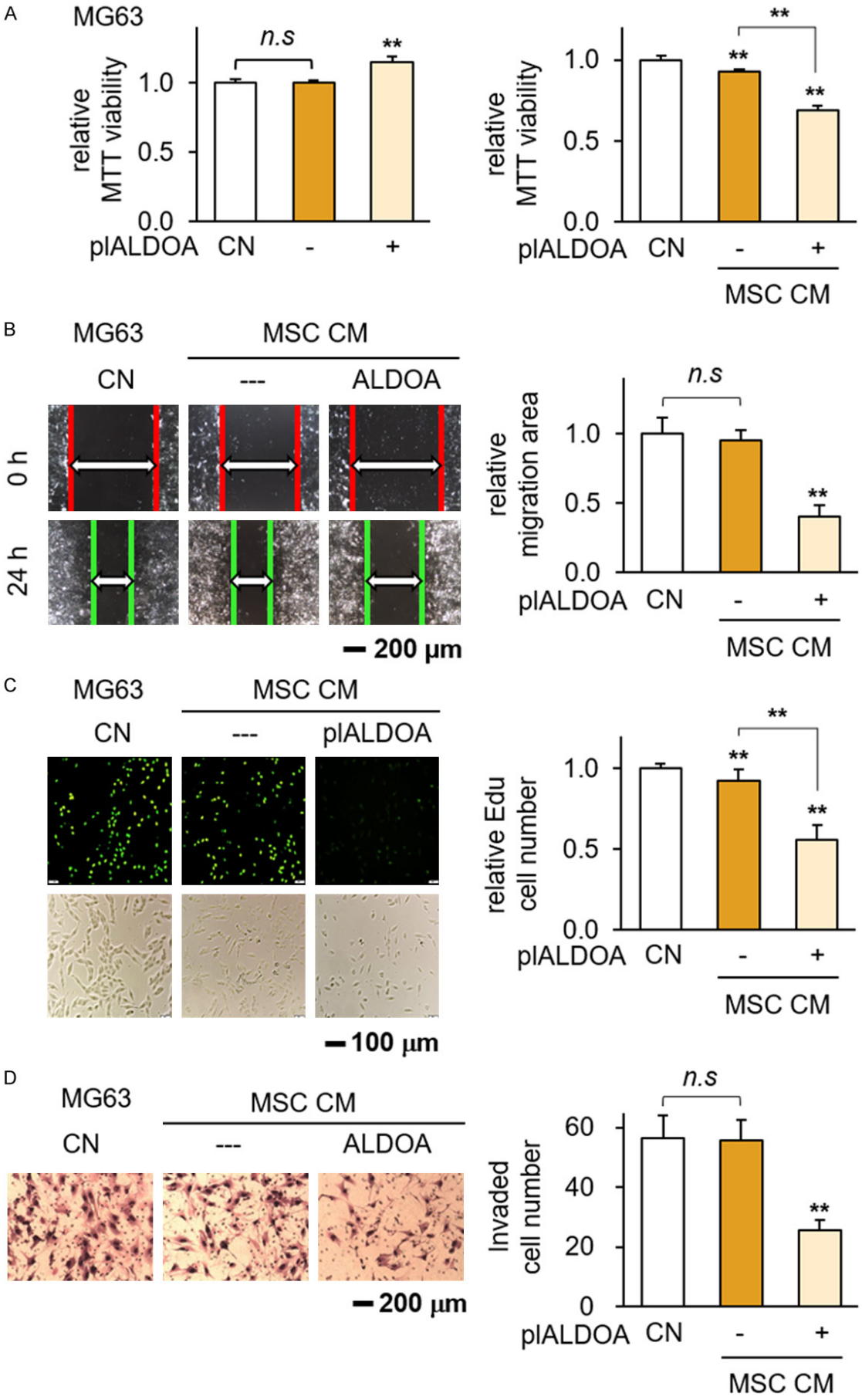
A
MG63
n.s
**
relative MTT viability
1.0
0.5
0.0
pIALDOA CN - +
**
**
**
relative MTT viability
1.0
0.5
0.0
pIALDOA CN - +
MSC CM
B
MG63
MSC CM
CN

ALDOA
0 h
24 h
200 μm
n.s
relative migration area
1.0
0.5
0.0
**
pIALDOA CN - +
MSC CM
C
MG63
MSC CM
CN
---
pIALDOA
100 μm
**
**
**
relative Edu cell number
1.0
0.5
0.0
pIALDOA CN - +
MSC CM
D
MG63
MSC CM
CN

ALDOA
200 μm
n.s
Invaded cell number
60
40
20
0
**
pIALDOA CN - +
MSC CM

Supplementary Figure 3. Tumor-suppressing role of ALDOA-overexpressing MSCs. CN = control, p = plasmid transfection, MSC = mesenchymal stem cell, and CM = conditioned medium. The double asterisk indicates P < 0.01. A. Contrasting role of ALDOA. The overexpression of ALDOA in MG63 OS cells elevated their MTT-based viability. However, ALDOA-overexpressing MSC-derived conditioned medium reduced the MTT-based viability of MG63 OS cells. B-D. Reduction in scratch-based motility, EdU-based proliferation, and transwell invasion, respectively, by ALDOA-overexpressing MSC-derived conditioned medium.

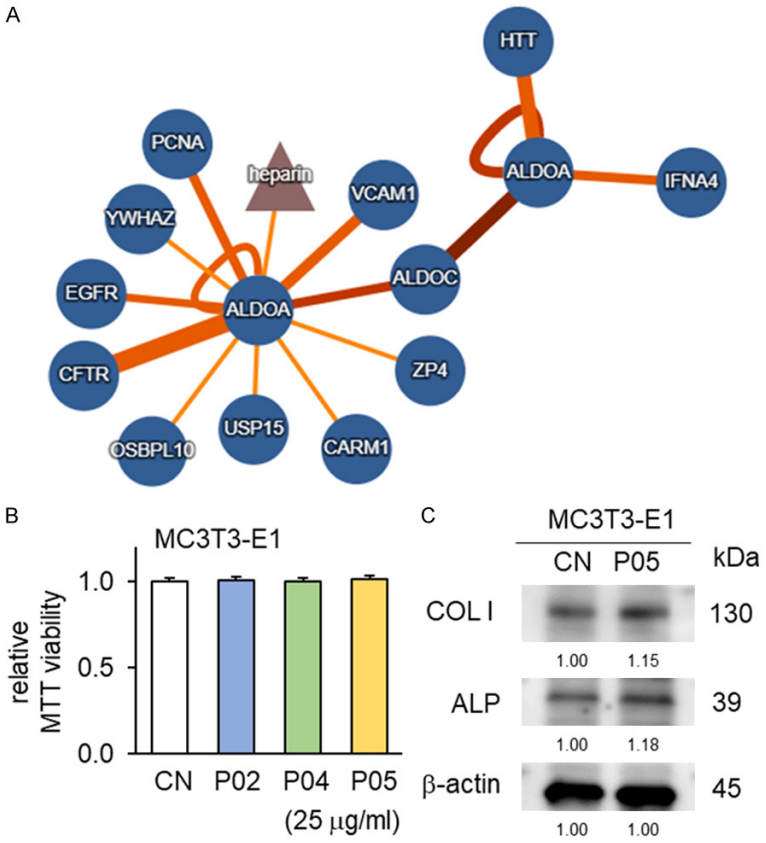

Supplementary Figure 4. Predicted network of the ALDOA-interacting protein candidates and the effect of P02, P04, and P05 on MC3T3-E1 osteoblast cells. A. Prediction of ALDOA-interaction protein candidates based on network. B. No significant change in the MTT-based viability of MC3T3-E1 cells in response to the administration of 25 μg/ml of P02, P04, or P05 peptides. C. Slight upregulation of type I collagen (COLI) and alkaline phosphatase (ALP) in response to the administration of 25 μg/ml of P05 peptides.

Supplementary Table 3. Hydrogen-bonding interaction in EGFR-ALDOA complex

EGFR Receptor Residue	ALDOA Ligand Residue	Interaction Constituents	Distance (A)	Type
C:ASN151	B:LYS28	B:LYS28:HZ2 - C:ASN151:OD1	2.3	Conventional
C:HIS359	B:LYS87	B:LYS87:HZ3 - C:HIS359:O	2.2	Conventional
C:GLU320	B:ASP89	B:ASP89:H - C:GLU320:O	2.6	Conventional
C:ASN91	B:GLY102	B:GLY102:H - C:ASN91:OD1	2.0	Conventional
D:VAL255	B:LYS330	B:LYS330:HZ1 - D:VAL255:O	2.7	Conventional
D:VAL255	B:LYS330	B:LYS330:HZ2 - D:VAL255:O	2.6	Conventional
C:SER146	B:GLN340	B:GLN340:HE21 - C:SER146:O	2.4	Conventional
D:PRO257	B:ALA352	B:ALA352:H - D:PRO257:O	2.6	Conventional
D:PRO257	B:ALA353	B:ALA353:H - D:PRO257:O	1.9	Conventional
C:TYR88	B:ASP68	C:TYR88:N - B:ASP68:OD2	2.8	Conventional
C:TYR88	B:ARG69	C:TYR88:OH - B:ARG69:O	3.2	Conventional
C:ASN314	B:LYS318	C:ASN314:ND2 - B:LYS318:O	2.6	Conventional
C:ASN331	B:ASP89	C:ASN331:ND2 - B:ASP89:O	3.1	Conventional
C:THR358	B:ASP90	C:THR358:OG1 - B:ASP90:O	3.0	Conventional
C:ASN151	B:LYS28	B:LYS28:HE3 - C:ASN151:OD1	1.9	Carbon
C:HIS359	B:LYS87	B:LYS87:HE2 - C:HIS359:O	3.0	Carbon
C:THR358	B:GLY91	B:GLY91:HA3 - C:THR358:O	2.5	Carbon
C:THR360	B:GLY91	B:GLY91:HA3 - C:THR360:OG1	2.0	Carbon
C:THR358	B:ARG92	B:ARG92:HA - C:THR358:O	2.8	Carbon
D:ASP254	B:ALA323	B:ALA323:HA - D:ASP254:OD2	2.4	Carbon
D:PRO257	B:GLU327	D:PRO257:CD - B:GLU327:OE2	2.6	Carbon
C:HIS334	B:ASP89	C:HIS334:CD2 - B:ASP89:OD1	3.7	Carbon

Supplementary Table 4. Hydrogen-bonding interaction in EGFR-P05 complex

EGFR Receptor Residue	P05 Ligand Residue	Interaction Constituents	Distance (A)	Type
A:CYS208	P05:ARG92	P05:ARG92:HH11 - A:CYS208:O	2.9	Conventional
A:GLN194	P05:ILE98	A:GLN194:CA - P05:ILE98:O	3.4	Carbon
A:SER196	P05:GLN96	A:SER196:CB - P05:GLN96:O	2.8	Carbon
A:HIS209	P05:ASP90	A:HIS209:CA - P05:ASP90:OD2	3.6	Carbon
B:GLN194	P05:ALA88	P05:ALA88:HA - B:GLN194:O	2.8	Carbon
A:GLU221	P05:GLY91	P05:GLY91:HA3 - A:GLU221:OE1	2.9	Carbon
A:SER196	P05:ARG92	P05:ARG92:HD2 - A:SER196:OG	2.4	Carbon
A:CYS208	P05:ARG92	P05:ARG92:HD3 - A:CYS208:O	1.9	Carbon
B:PRO219	P05:PRO95	P05:PRO95:HA - B:PRO219:O	2.1	Carbon
B:PRO219	P05:PRO95	P05:PRO95:HD3 - B:PRO219:O	2.6	Carbon